



Influence of water extraction on subglacial hydrology and glacier velocity

Colin R. Meyer¹, Katarzyna L. P. Warburton², Aleah N. Sommers¹, and Brent M. Minchew^{3,4}

Correspondence: Colin R. Meyer (colin.r.meyer@dartmouth.edu)

Abstract. Subglacial water modulates glacier velocity across a wide range of space and time scales by influencing friction at the glacier bed. Observations show ice acceleration due to supraglacial lake drainage and water draining through moulins, where both configurations involve water inputs to the bed. Here we consider the reverse: water extraction from the subglacial system. Removing subglacial water results in different dynamics than injecting water, and we hypothesize that understanding these processes will allow for improved characterization of the physics of subglacial hydrology. Water extraction is a proposed intervention method for slowing glaciers that requires significant further investigation before it should be tested or implemented in the field. Here we set up model experiments in the Subglacial Hydrology And Kinetic, Transient Interactions (SHAKTI) model coupled with the Ice-sheet and Sea-level System Model (ISSM). By analyzing the problem of an isolated borehole in a background pressure field to determine the region of extraction influence, we find an analytical solution which shows that the water pressure returns to the background value approximately as a logarithm with distance. The benefit of the analytical solution is that the dependence of uncertain parameters is clear and may be used to constrain subglacial hydrology models. We find good agreement between this analytical result and full SHAKTI simulations. Using the coupled SHAKTI-ISSM model, we perform transient model experiments on an idealized tidewater glacier geometry and on Helheim Glacier in Greenland to determine the effects of water extraction on glacier velocity. With continuous pumping, we simulate a modest impact on velocity, which is sensitive to the extraction rate and site location. The response time to pumping initiation and the recovery time following cessation scale according to effective pressure, with typical times on the order of hours to days. These results are encouraging that water extraction is a method of probing the subglacial hydrologic system to better constrain the uncertain physics, with further research required to determine if it is an effective intervention method.

1 Introduction

Water flowing beneath glaciers influences ice velocity on short (e.g. daily) to longer (e.g. seasonal, annual, decadal) timescales. For mountain glaciers that primarily flow over bedrock, water flow along the ice-bed interface pressurizes cavities and can coalesce into channels (Kamb, 1987; Hewitt, 2011; Flowers, 2015). For ice streams and outlet glaciers, such as the Siple Coast

¹Thayer School of Engineering, Dartmouth College, Hanover, NH 03755 USA

²Department of Applied Mathematics and Theoretical Physics, University of Cambridge, CB3 0WA, UK

³Department of Earth, Atmospheric and Planetary Sciences, Massachusetts Institute of Technology, Cambridge, MA 02142, USA

⁴Seismological Laboratory, California Institute of Technology, Pasadena, CA 91125, USA



35



Ice Streams in Antarctica or Helheim Glacier in southeast Greenland, nearly all of their motion comes from slip at the base, where ice flows over water-saturated sediment (Alley et al., 1986; Kamb, 2001; Minchew and Joughin, 2020; Stevens et al., 2022a). In both cases, water at the ice-bed interface can act as a lubricant, allowing glaciers to accelerate. Fast glacier slip also produces water as frictional heating melts the ice, potentially initiating a positive feedback (Schoof and Mantelli, 2021). Effective pressure, defined as the local difference between ice weight and water pressure, is a key control on glacier sliding speed. At low effective pressure (high water pressure) additional water leads to glacier acceleration whereas in higher effective pressure regions (lower water pressure), additional water reduces glacier velocity due to increased efficiency in water flux (Zwally et al., 2002; Schoof, 2010). On shorter time-scales, glaciers respond to the sudden addition of water from the drainage of supraglacial lakes and streams into moulins. Here water is added at a rate much faster than the subglacial hydrological network adapts, leading to localized acceleration (Das et al., 2008; Andrews et al., 2014; Stevens et al., 2016; Mejía et al., 2021, 2022; Stevens et al., 2022b). Understanding the response of glaciers to meltwater is an ongoing challenge as climate changes and glaciers recede, accelerate, and decay.

In the context of disappearing glaciers and sea-level rise, researchers have proposed ways of conserving glacier ice, i.e., intervention strategies that mitigate ice mass loss due to climate change (Moore et al., 2018), and these ideas have rightly sparked debate (e.g., Moon, 2018; Carey et al., 2022; Flamm and Shibata, 2025; Siegert et al., 2025). One proposed mechanism to slow the speed of glaciers is to extract water from beneath glaciers in an effort to increase the subglacial effective pressure (i.e. lower the subglacial water pressure), thereby increasing the subglacial friction and reducing glacier velocity (e.g., Lockley et al., 2020). Although this idea could have merit at glaciers where the velocity response to added meltwater is acceleration, it would likely not work in locations with efficient drainage. Siegert et al. (2025) describe a host of issues with subglacial pumping as an intervention strategy and indicate that significant further research is required before further consideration. We agree: the focus of this paper is to understand the impact of water exaction on subglacial hydrology in a model.

A natural analog for intervention in subglacial hydrology is the seasonal addition of meltwater. Observations of glacier velocity in Greenland show seasonal variation, driven by surface melt reaching the subglacial hydrologic system (Moon et al., 2014; Vijay et al., 2019; Solgaard et al., 2022). The meltwater driven seasonal patterns have frequently been categorized into two responses. For type-I glaciers, the velocity increases with meltwater, with the highest velocities observed in summer. In this case, additional meltwater decreases friction, and allows for faster glacier sliding. For type-II glaciers, meltwater input reduces the glacier velocity, indicating that adding water to these subglacial environments increases the friction by developing a channelized network that efficiently drains the bed. In terms of subglacial water pressure, adding meltwater increases water pressure for type-I glaciers over the course of the melt season, and decreases water pressure for type-II glaciers. As a glacier intervention strategy, extracting water from a type-I glacier should theoretically reduce its velocity, but may have the opposite effect on a type-II glacier when considering mean annual velocity. Although a glacier may respond as type-I or -II in aggregate, the subglacial hydrologic system below glaciers is heterogeneous and the physical processes that control whether a glacier will respond to water extraction are largely unknown.

With only sparse direct observations of subglacial water pressure, subglacial hydrology models offer a way to understand controls on effective pressure and sliding (Flowers, 2015; de Fleurian et al., 2018). The Glacier Drainage System (GlaDS)



65



model has been applied to numerous glacier systems to simulate the evolution of water pressure (e.g. Werder et al., 2013; Poinar et al., 2019; Dow et al., 2022; Ehrenfeucht et al., 2025). The Subglacial Hydrology and Kinetic, Transient Interactions (SHAKTI) model is a continuum model that has also been applied to numerous glaciers to determine the subglacial conduit geometry and local effective pressure (e.g. Sommers et al., 2018, 2023; Narayanan et al., 2025). By coupling SHAKTI to the Ice-sheet and Sea-level System Model, Sommers et al. (2024) simulated Helheim Glacier to determine the realm of influence of the terminus as compared to regions dominated by hydrology. Here we use the SHAKTI model, but focus on advances that generalize to all subglacial hydrology models.

Pumping water into and out of groundwater aquifers is a standard technique for characterizing permeability, among other properties. Consider a groundwater system with an aquifer at some depth below the surface. As water is extracted (input), the height of the aquifer is lowered (raised), indicating a decrease (increase) in hydraulic head, i.e. the ratio of water pressure to specific gravity, $h = p_w/(\rho_w g)$. In the case of extraction, the flow results in a reduction of hydraulic head that propagates outward as a similarity solution known as the Theis solution, with the radial coordinate scaling with time like $r \sim t^{1/2}$ (Fitts, 2002). If there is recharge in the system, i.e. water flow into the region during pumping, the solution approaches a steady balance between recharge and extraction. The Theis method was used to characterize a deep subglacial groundwater system in Greenland (Liljedahl et al., 2021) where they found stratigraphic layers with differing permeability. Building on the strong foundation of understanding of water extraction in groundwater hydrology, our aims here are to (i) similarly characterize the subglacial hydrologic system by its response to water extraction and (ii) to derive a solution analogous to the Theis solution to serve as a starting point for model, lab, and potentially field tests.

Although we are not aware of any studies probing the subglacial environment via water extraction, measuring the response to water input has been tried and analyzed, such as in the field experiments by Engelhardt and Kamb (1997, 1998). In a series of drilling campaigns on the Siple Coast, Antarctica, these researchers used hot water to drill holes to the bed of numerous glaciers. They measured the water pressure as the hot-water drilling fluid connected to the subglacial system and equilibrated. Then they used the pressure pulse to determine the effective permeability of the subglacial system. Characterizing the permeability as an effective water layer thickness, they found that it was on the order of 2 mm. Engelhardt et al. (1990) found water pressure to be near or slightly above the overburden ice pressure. These findings are consistent with work by Alley (1996), Weertman and Birchfield (1982), and Doyle et al. (2022).

In this paper, we analyze the effects of extracting water on the subglacial environment through mathematical analysis and computational modeling. In the following sections, we start by analyzing the results of a simulation pumping at a single location on Helheim Glacier in southeast Greenland, as motivation. We develop analytical and numerical solutions, showing the radius of influence of water extraction and response time to pumping. Next, we return to coupled SHAKTI-ISSM numerical simulations at Helheim, with multiple extraction sites. Then, we provide context for our results in terms of glacier intervention and discuss next steps. Finally, we end with conclusions and recommendations for further research.





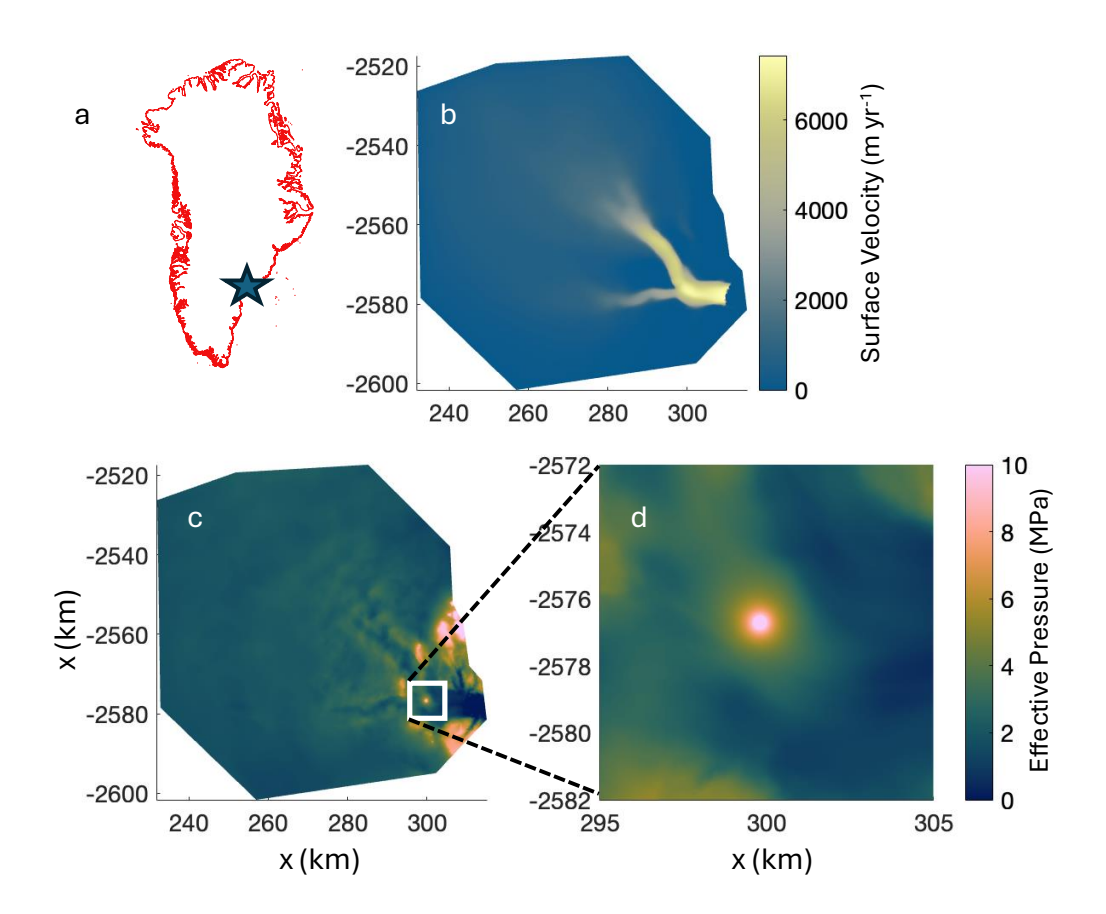


Figure 1. Simulation context: (a) Location of Helheim Glacier in southeast Greenland. (b) Ice surface velocity on model domain. (c) and (d) Pumping test simulation at a single extraction site near the confluence of the two main branches, with a pumping rate of 1 m³/s, shows high effective pressure around the pumping site. All x and y coordinates throughout the figures are given in Polar Stereographic North projection.

90 2 Approach

Here we describe the setting and rationale for our numerical simulations. We focus on Helheim Glacier, a large, marine-terminating outlet glacier in southeast Greenland. The location of Helheim and the simulation domain are shown in figure 1a,b. Helheim is among the largest contributors to sea-level rise from glaciers in Greenland (Mankoff et al., 2020), moving several km per year in its main trunk as shown in Fig. 1c.

For these simulations, we use the Subglacial Hydrology And Kinetic, Transient Interactions (SHAKTI) model built into the Ice-sheet and Sea-level System Model (ISSM). SHAKTI-ISSM simulations have previously been conducted on Helheim Glacier (Sommers et al., 2023, 2024), yielding an established model environment for extraction testing to analyze the efficacy of interventions in slowing a fast-moving glacier. The subglacial hydrology model can either be run with fixed ice dynamics or be two-way coupled to the ice dynamics through the basal stress (i.e. friction parameterization or sliding law) as in Sommers





et al. (2024). When coupled, variations in sliding velocity affect pressure and vice versa: frictional heat generated by sliding over the bed leads to enhanced melt and the resulting subglacial effective pressure (i.e., ice overburden less water pressure) is incorporated into the sliding law, which affects the velocity dynamics of the glacier flow. We use a Budd-type sliding law of the form

$$\tau_b = C^2 u_b N,\tag{1}$$

where N is the effective pressure, calculated by SHAKTI, u_b is the subglacial sliding velocity calculated by the stress balance in ISSM, τ_b is the subglacial shear stress, and C^2 is the drag coefficient.

SHAKTI solves for a gap height b that is a continuum quantity, representing a distributed, channelized, or thin-film region (Sommers et al., 2018), i.e.

$$\frac{\partial b}{\partial t} = \frac{\dot{m}}{\rho_i} - A|N|^{n-1}Nb, \qquad \text{gap height evolution}$$
 (2)

 $q = \frac{-b^3}{12\mu \left(1 + \omega \frac{|q|}{\nu}\right)} \nabla N, \qquad \text{subglacial water flux}$ (3)

$$\dot{m}\mathcal{L} = G + u_b \tau_b - \boldsymbol{q} \cdot \boldsymbol{\nabla} N,$$
 energy conservation (4)

$$\nabla \cdot \mathbf{q} = \dot{m} \left(\frac{1}{\rho_w} - \frac{1}{\rho_i} \right) + A|N|^{n-1}Nb + i_{eb}, \qquad \text{mass conservation}$$
 (5)

$$N = \rho_i g H - p_w,$$
 effective pressure (6)

with melt rate \dot{m} , ice softness A, geothermal flux G, water flux q, subglacial water pressure p_w , basal friction τ_b , basal velocity u_b , and input of meltwater into the system from englacial or surface sources i_{eb} . Here $|q|/\nu$ is the local Reynolds number and ω is a friction factor, parameterizing the Reynolds number at which transition to turbulence occurs. For fully turbulent flow, $q \propto \sqrt{\nabla h}$. Consistent with Sommers et al. (2024), we neglect opening by sliding due to cavities, pressure melting, and transient englacial storage of meltwater (cf. Creyts and Schoof, 2009; Robel et al., 2013; Kyrke-Smith et al., 2014; Brinkerhoff et al., 2016; Rempel et al., 2022). We also take the Glen's law exponent to be n=3. We impose no flux boundary conditions on all edges, except the terminus where we match the ocean water pressure at the bottom of the fjord to the subglacial water pressure. We start by running under background "winter conditions" simulation, where no surface meltwater is input ($i_{eb}=0$) and we find a steady state, with all subglacial water produced through basal melt.

Our first experiment perturbed this steady state by extracting water at a constant rate Q from one location near the confluence of the two primary branches of Helheim. We implement this extraction flux in the same way as a moulin inputs water to the bed, except with a negative sign indicating that water is leaving the subglacial system. Later in the paper we consider extracting from multiple locations at the same time. In our initial tests of the single borehole case, we immediately found that if we extracted too much water (i.e., $Q \gtrsim 2$ m³/s), the simulations would crash due to insufficient available water. The extraction well could not recharge fast enough. Taking Q = 1 m³/s, we show the effective pressure distribution in figure 1d,e, including both the entire simulation domain and an enlarged view around the extraction borehole.

Motivated by these simulation results, we would like to answer three primary questions about extracting water from the subglacial system:





SHAKTI parameters				variable scales		nondimensional	
ρ_i	917 kg m^{-3}	g	$9.80~{\rm m~s^{-2}}$	[b]	0.152 m	R	8.91×10^{-4}
$ ho_w$	$1000~\rm kg~m^{-3}$	μ	1.8×10^{-3} Pa s	[N]	200 kPa	M	4.90×10^{-7}
$u_b \tau_b$	$0.08~{ m W}~{ m m}^{-2}$	G	$0.05~\mathrm{W~m^{-2}}$	[r]	10 km	D	2.45×10^{-4}
A	$3.5 \times 10^{-25} \; \mathrm{s^{-1} \; Pa^{-3}}$	n	3	[t]	11 yr	\hat{D}	1900
\mathscr{L}	$3.34 \times 10^5 \; \mathrm{m^2 \; s^{-2}}$	ω	0.001	r_t	8.9 m	W	2.45
Q	$1 \text{ m}^3 \text{ s}^{-1}$	N_0	200 kPa				
r_d	10 km						

Table 1. Table of parameters and representative values for SHAKTI simulations.

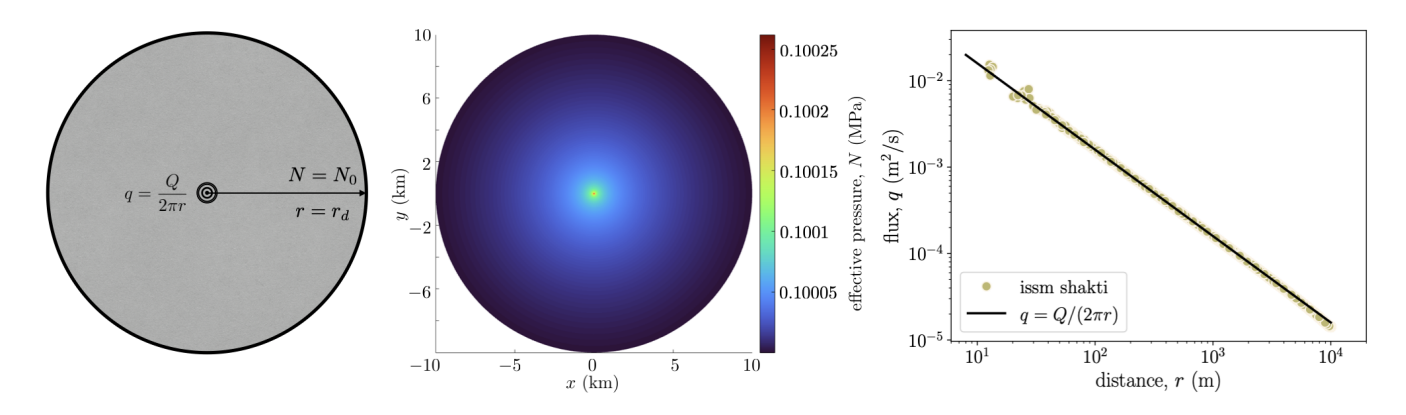


Figure 2. Asymmetric model: (left) schematic showing water extraction at the origin and a fixed effective pressure boundary condition at the outer edge. (middle) SHAKTI-ISSM results for the effective pressure in a 10 km domain. (right) water flux results from SHAKTI-ISSM showing that the flux goes like 1/r throughout the entire axisymmetric domain.

- 1. What is the radius of influence of an extraction borehole?
- 2. What is the effective pressure at the location of extraction?
- 3. How long does it take to reach a new steady state while pumping?

These questions are crucial for characterizing the hydrologic response to water extraction in the laboratory or field, and for inferring the hydrological system from such tests. We need to know what magnitude of pressure change we expect to see, how far it will propagate, and how long it will take to equilibrate. These questions will also inform the potential efficacy of intervention.

Based on the simulation results shown in figure 1d,e, we find that the effective pressure distribution around the borehole is close to axisymmetric. In order to gain more insight into the solution structure and verify our numerical simulations, we now describe a reduced model for water extraction in an axisymmetric geometry.





3 Axisymmetric model

Inspired by the single-borehole, water-extraction simulations at Helheim, we consider the axisymmetric pressure response to pumping water out of the subglacial system at a constant volume flux Q. Water conservation, equation (5), would allow us to solve for the structure of q(r) around the borehole, but in this section we assume that close to the borehole only a negligible contribution comes from local melt, such that

$$q = \frac{Q}{2\pi r}. (7)$$

The SHAKTI domain, effective pressure results, and water flux are shown in figure 2.

Writing the water flux as in equation (7) allows us to simplify equation (3) to

150
$$\frac{Q}{2\pi r} \left(1 + \frac{\omega Q}{2\pi \nu r} \right) = -\frac{b^3}{12\mu} \frac{\partial N}{\partial r}.$$
 (8)

The time-dependent gap height equation is given by

$$\frac{\partial b}{\partial t} = \frac{\dot{m}}{\rho_i} - AN^3b. \tag{9}$$

The melt rate \dot{m} is given by

$$\dot{m}\mathcal{L} = G + u_b \tau_b - \frac{Q}{2\pi r} \frac{\partial N}{\partial r}.$$
 (10)

The variables are b, N, t, r and the boundary conditions are $N = N_0$ at $r = r_d$ and the imposed flux Q at r = 0. The initial condition is b = [b] f(r) at t = 0.

We scale the variables as

$$b = [b]b^*, \quad t = [t]t^*, \quad r = [r]r^*, \quad N = N_0 N^*, \quad \dot{m} = \frac{G + u_b \tau_b}{\mathscr{S}} \dot{m}^*,$$

where the brackets are the size of the variables we choose momentarily. Nondimensionalizing allows us to write the three equations as

$$M\left(\frac{1}{r^*} + \frac{R}{r^{*2}}\right) = -b^{*3}\frac{\partial N^*}{\partial r^*},\tag{11}$$

$$\dot{m}^* = 1 - \frac{D}{r^*} \frac{\partial N^*}{\partial r^*},\tag{12}$$

$$\frac{\partial b^*}{\partial t^*} = \dot{m}^* - N^{*3}b^*, \tag{13}$$

with the initial and boundary conditions

65
$$N^* = 1$$
 at $r^* = 1$ and $b = f(r^*)$ at $t^* = 0$.

where we choose that

$$[t] = \frac{1}{AN_0^3}, \quad [b] = \frac{G + u_b \tau_b}{\rho_i \mathcal{L} AN_0^3}, \quad [r] = r_d, \quad r_t = \frac{\omega Q}{2\pi\nu},$$





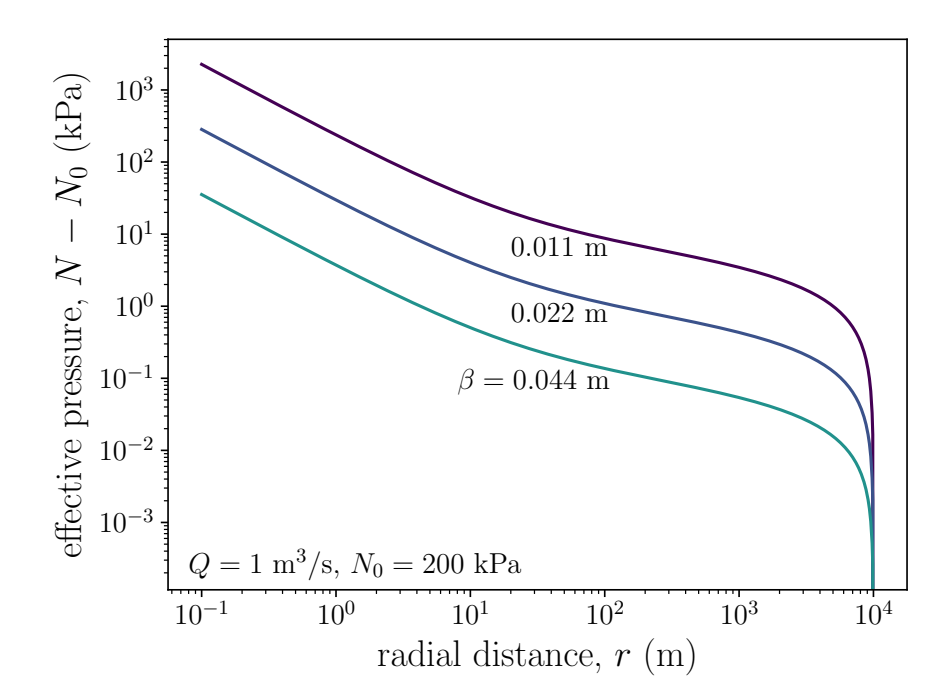


Figure 3. Effective pressure enhancement due to water extraction with a constant gap height. The domain is a 10 km circle and water is extracted from the center, with a flux given as $q = Q/(2\pi r)$. For the smallest gap height shown, the effective pressure at the extraction site exceeds 1 MPa above the background value.

and we can write

$$R = \frac{\omega Q}{2\pi\nu[r]} = \frac{r_t}{r_d} \sim 10^{-2}, \quad M = \frac{12\mu Q}{2\pi[b]^3 N_0} \sim 10^{-3}, \quad D = \frac{QN_0}{2\pi[r]^2 (G + u_b \tau_b)} \sim 10^{-3}.$$

The scale for the numbers comes from reasonable parameter values, cf. table 1. We can see that R, M, and D are all small parameters. We exploit the smallness of D in the next section and derive a solution that ignores the role of turbulent dissipation on melting. Based on the equation structure, however, we can notice that as r becomes small ($r \sim D$) and $\partial N/\partial r$ becomes large, this approximation will fail.

3.1 Radius of influence

175

3.1.1 Solution for constant gap height

A starting point to understand the dynamics of water extraction is to consider the case where the gap height is constant, $b = \beta$. Although this limit is somewhat artificial, it is relevant to the initial pumping dynamics, i.e. before the system reaches a steady state, and it is relevant to the SHAKTI simulations of Helheim. In this limit, equation (11) becomes

$$\frac{dN}{dr} = -\frac{M}{\beta^3} \left(\frac{1}{r} + \frac{R}{r^2} \right),\tag{14}$$



190



where we have rearranged and dropped the asterisks. In this case, the gap height in the region around the extraction site will not evolve with time, and the effective pressure response will also be independent of time. Integrating and applying the boundary condition at the outer edge, i.e. N = 1 at r = 1, we find that

$$N = 1 - \frac{M}{\beta^3} \left(\ln(r) + R - \frac{R}{r} \right). \tag{15}$$

In this way, the effective pressure response is akin to a porous medium, where the β^3 term represents a constant permeability.

We plot the analytical solution for the effective pressure as a function of r in figure 3. The effective pressure near the point of extraction is significantly enhanced as compared to the background value.

In figure 4, we revisit the SHAKTI pumping simulations in the confluence region of Helheim Glacier, Greenland, as shown in figure 1. We see that the constant gap height solution works well to explain the effective pressure near the water extraction site, due to the axisymmetric flux and fixed value of b. As we discuss later in the paper, the SHAKTI simulations at Helheim do not always evolve the gap height in time. In the next section, we see that the connection between effective pressure and gap height turns out to be important in determining the effective pressure at the pumping location.

3.1.2 Far-field solution ignoring melt from dissipation

To understand the dynamics far away from the extraction site, we return to equations (11)-(13). We initially neglect dissipation in the water flow, yielding

195
$$M\left(\frac{1}{r} + \frac{R}{r^2}\right) = -b^3 \frac{\partial N}{\partial r},$$
 (16)

$$\frac{\partial b}{\partial t} = 1 - N^3 b, \tag{17}$$

where we have again dropped the asterisks. To solve these equations, we employ a relaxation method: we use forward Euler to march the gap height b forward in time and then integrate for N as a numerical definite integral, until we reach a steady state.

We can also derive the steady state solution analytically. When the gap height no longer changes with time, we have

$$200 N^3 b = 1, (18)$$

which we can combine with the flux equation to give that

$$M\left(\frac{1}{r} + \frac{R}{r^2}\right) = -N^{-9}\frac{\partial N}{\partial r} \tag{19}$$

Integrating and applying the boundary condition, we find that

$$N = \left[1 + 8M\left(\ln(r) + R - \frac{R}{r}\right)\right]^{-1/8}.$$
 (20)

As we show in figure 5, this solution is a good approximation of the effective pressure far from the extraction location, which is consistent with our intuition about neglecting the dissipation term. Examining the near-field of equation (20), we see a singularity in N when the denominator approaches zero, which happens approximately at

$$r \sim 8MR,$$
 (21)





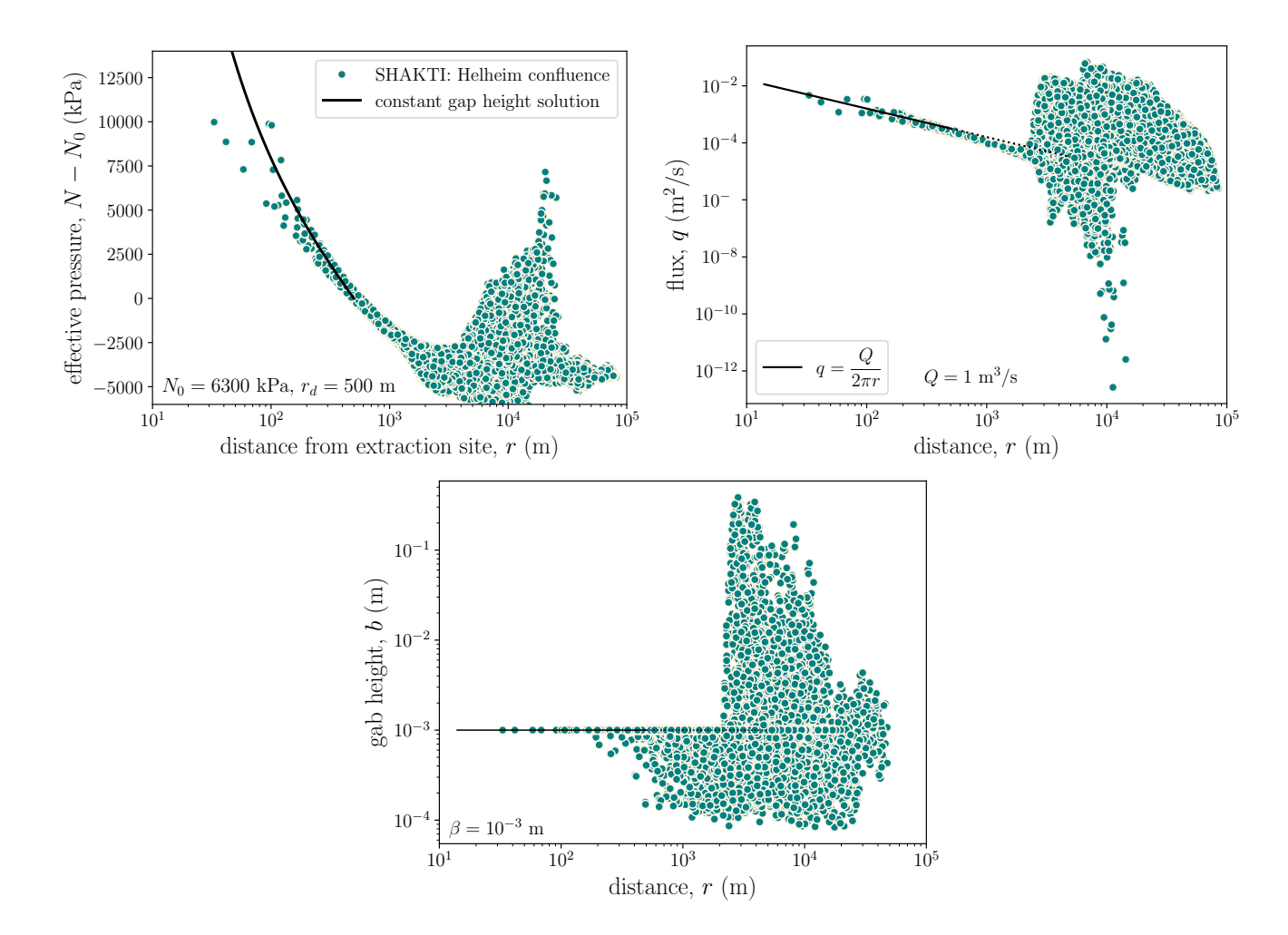


Figure 4. SHAKTI results and constant gap height model for the pumping tests in the confluence region of Helheim Glacier. (left) effective pressure follows the analytical solution, equation (15) near the extraction site; (middle) flux decays like $Q/(2\pi r)$; and (right) the gap height is nearly constant close to the pump.





In the far-field of equation (20), where the flow is laminar, i.e. $r \gg R$, and dominated by melt from geothermal flux, we have

$$N = [1 + 8M \ln(r)]^{-1/8}. (22)$$

The logarithmic dependence on r implies that the effective pressure is larger than the background value throughout the entire domain but with diminishing magnitude. This is shown in figures 2 and 5. In particular, in figure 5, we compare the SHAKTI-ISSM simulations to the analytical solution (20) and a steady ODE solution to the axisymmetric equations where we do not ignore dissipation, which we describe in the next section.

215 3.1.3 Full domain solution including dissipation

If we now include the effect of turbulent dissipation on melting, which becomes important as q increases towards the borehole, we must solve the full set of equations numerically. We adapt the same relaxation method, where we use the value of the gap height at the previous time step to find $\partial N/\partial r$ from the equation for the water flux. We then use $\partial N/\partial r$ to find the melt rate, and use that expression to move forward in time and update b.

220 In steady state, we have the reduced equations given by

$$M\left(\frac{1}{r} + \frac{R}{r^2}\right) = -b^3 \frac{\partial N}{\partial r},\tag{23}$$

$$N^3b = 1 - \frac{D}{r} \frac{\partial N}{\partial r}.$$
 (24)

We can combine these into a single ODE for $\partial N/\partial r$ as

$$\left[1 + \frac{D}{r}\left(-\frac{\partial N}{\partial r}\right)\right]^3 \left(-\frac{\partial N}{\partial r}\right) = \frac{M}{r}\left(1 + \frac{R}{r}\right)N^9,\tag{25}$$

225 where we solve for $-\partial N/\partial r$ using a root-finding algorithm and then integrate backward starting from N=1 at r=1.

As shown in figures 2 and 5, the largest pressure perturbations occur close to the extraction site, where the flow velocity is turbulent. The distance from the borehole where the flow becomes laminar is $\sim r_d R \sim 200$ m. Due to the logarithmic dependence of the outer solution, i.e., equation (22), there are pressure perturbations out to the edge of the domain. In this model, the full radius of influence is the distance away when q is no longer axisymmetric, which depends on the strength of the fluid flow in the existing subglacial hydrologic system. Near the borehole, we see that the dissipation regularizes the singularity in equation (20). The gap height field is dominated by turbulent melting in the near field and decays to a constant ($b \sim [b]$) in the far field. These results differ from the constant gap height solution, i.e., equation (15) and figure 3, in that the effective pressure enhancement at the extraction site is modest.

3.2 Effective pressure at extraction location

230

To answer the question of how large is the effective pressure at the extraction site, we numerically solve the steady ODE that includes turbulent dissipation, i.e., equation (25), as described in the previous section. Unlike the approximate analytical solution, where is there is a singularity as $r \to 8MR$, including dissipation regularizes the singularity and the near-field effective





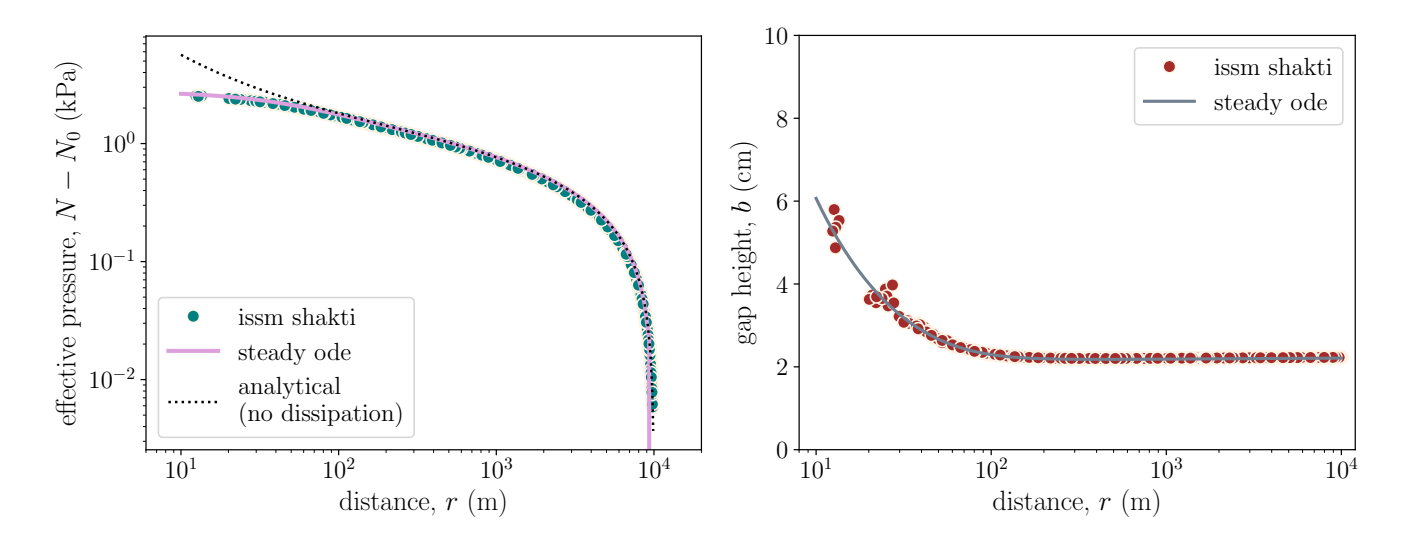


Figure 5. Idealized numerics with $Q = 1 \text{ m}^3 \text{ s}^{-1}$ and $N_0 = 200 \text{ kPa}$. (left) comparison of steady state numerical ODE solution, SHAKTI-ISSM, and a reduced model with radial distance. (right) gap height as a function of radius, showing turbulent melting near the borehole.

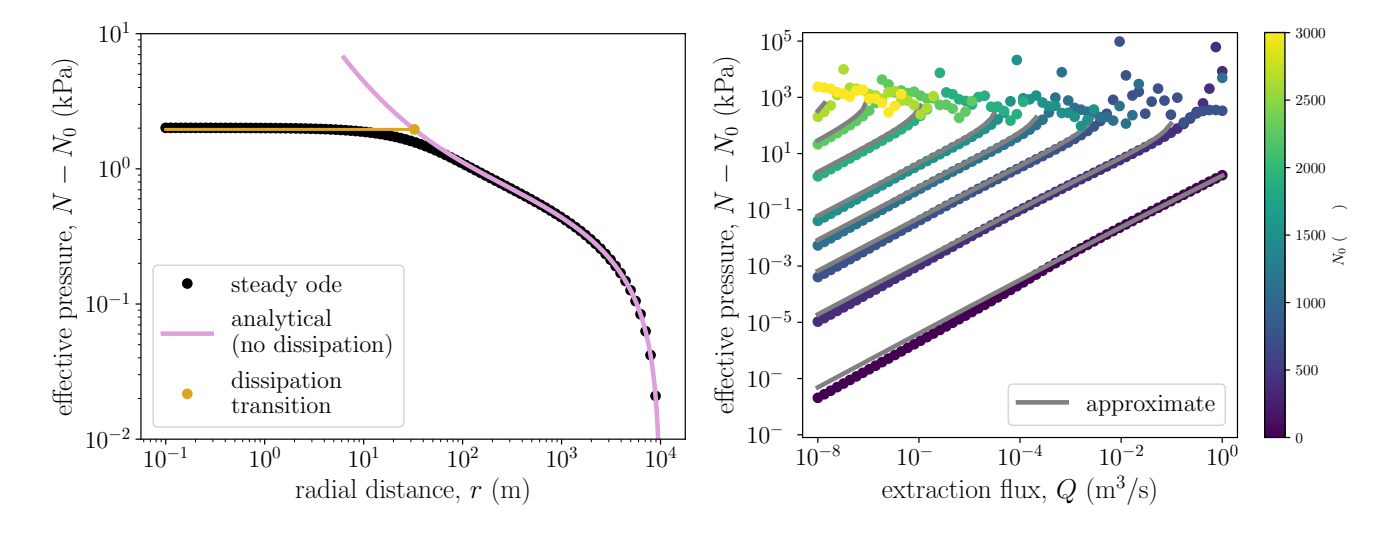


Figure 6. In steady state, extracting water increases the local effective pressure by stimulating water flow: (left) effective pressure as a function of radial distance, showing the analytical solution where we ignore dissipation. (right) Using axisymmetric, fixed-flux ODE form of SHAKTI, we determined the effective pressure at the borehole as a function of the extraction flux Q for many different initial effective pressures. By finding the radius where turbulent dissipation is significant, we approximate the effective pressure at the borehole (gray curves) from equation (29).



245

255

260

265



pressure approaches a constant. In figure 6, we can see the steady ODE solution to the problem, showing the approach to a constant in the near field, the singularity in the approximate analytical expression, and the logarithmic decay behavior in the 240 far field.

Based on these results, we can see that there is a boundary layer for small r where turbulent dissipation dominates, the gap height opens due to enhanced melting, and the effective pressure is more or less constant. Matching this inner region to the approximate analytical outer solution, equation (20), proved intractable analytically, in part because of the singularity at finite r. To capture the essence of the behavior, we noticed that the value of effective pressure for the outer solution at the point where the dissipation is order unity, i.e.

$$-\frac{D}{r}\frac{dN}{dr} \sim 1,\tag{26}$$

is close to the value of the inner solution. In this region, we assume that r < R, so that the effective pressure and its gradient are approximately given as

$$N \simeq 1 + \frac{MR}{r}$$
 and $\frac{dN}{dr} \simeq -\frac{MR}{r^2}$. (27)

250 This implies that the dissipation term is order unity when the radius r is approximately

$$r \simeq (DMR)^{1/3} \,. \tag{28}$$

We then evaluate the outer effective pressure analytical expression at this radius and find that

$$N \simeq 1 + \left(\frac{M^2 R^2}{D}\right)^{1/3} \tag{29}$$

As shown in figure 6, this approximate approach agrees well with the full solution. The value of the effective pressure at the borehole is a function of the extraction flux, Q. The approximate solution captures this relationship nicely, although it starts to diverge slightly for large fluxes. Large pump systems could potentially be deployed on a glacier to pump on the order of $1-10 \text{ m}^3/\text{s}$, and these fluxes yield effective pressure changes on the order of 1-10 kPa. In the context of the chosen parameters, the effective pressure values are about 1-10% of the background effective pressure, which is a small fraction of the total. If the boundary effective pressure is large, however, this solution breaks down, which we discuss in the next section. These general predictions are for a steady state model that does not include positive feedbacks involving sliding, melt generation, and freezing.

3.2.1 Pressure divergence at high pumping rates

As the value of the outer effective pressure becomes larger in figure 6, we see that there is a breakdown in the numerical solution, which almost uniformly occurs for large effective pressures. To understand this breakdown, we look for the domain of applicability for equation (25). To start, we can see that as the effective pressure at the outer boundary increases, the hydraulic permeability of the domain decreases. For a fixed form of the flux $q = Q/2\pi r$, this means the pressure gradient towards the borehole must increase to maintain the imposed value of Q, further increasing N and decreasing the gap height



270

275



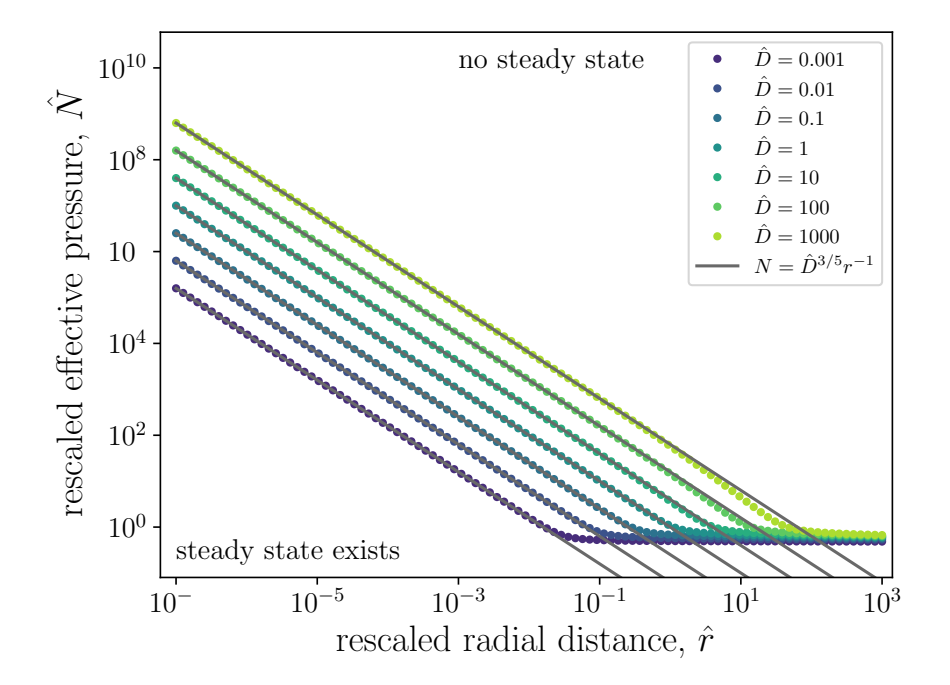


Figure 7. Curves of maximum steady state effective pressure as a function of radial distance and a unified dissipation parameter \hat{D} . Choosing initial conditions at a radius below the curve for a given \hat{D} result in a steady solution, whereas steady solutions above the curve do not exist.

and permeability. If the outer boundary pressure is too large for the flux imposed, the effective pressure diverges before the before we reach r=0. Physically, this corresponds to a hydrological system that collapses in on itself from the induced pressure gradients, like a straw collapsing shut. Indeed, for any value of Q and domain size r_d we can find the maximum N_0 at the boundary such that this divergence occurs exactly at r=0. Since $\partial N/\partial r$ is only a function of N and r, considering this as a 2D dynamical system, curves of N(r) cannot intersect, so any solutions with a lower value of N_0 will remain bounded as $r\to 0$ and any with a larger value of N_0 will diverge at finite r. Practically, it is easiest to integrate outwards from r=0, and continue along this bounding curve, which we refer to as the envelope, to reach any value of r_d .

We start by rescaling the variables so that

$$r = R \hat{r}, \quad N = M^{-1/8} \hat{N}, \quad \text{and} \quad \hat{D} = \frac{D}{R^2 M^{1/8}} = \frac{(2\pi)^{9/8} \nu^2}{(12\mu)^{1/8} (\rho_i LA)^{3/8} (G + u_b \tau_b)^{5/8} \omega^2 Q^{9/8}},$$

which is independent of N_0 and r_d . This rescaling leads to a one-parameter version of equation (25), i.e.

$$\left[1 + \frac{\hat{D}}{r} \left(-\frac{\partial \hat{N}}{\partial \hat{r}}\right)\right]^3 \left(-\frac{\partial \hat{N}}{\partial \hat{r}}\right) = \frac{1}{\hat{r}} \left(1 + \frac{1}{\hat{r}}\right) \hat{N}^9,\tag{30}$$

which has an asymptotic solution for small \hat{r} of $\hat{N} \simeq \hat{D}^{3/5}\hat{r}^{-1}$. We integrate equation (30), starting from a very large effective pressure at the extraction site (i.e., $\hat{N} = D^{3/5}/\epsilon$ at $\hat{r} = \epsilon$ with $\epsilon \to 0$) and find that the curve locks onto the largest steady state effective pressure for given values of \hat{r} and \hat{D} . The result of this integration is shown in figure 7. The different curves on the



285



plot in figure 7 represent different values for the parameter \hat{D} , corresponding different extraction fluxes Q, and parameters such as ice softness A and geothermal heat G. From this analysis, we can see that if we impose $N=N_0$ at a radius $r=r_d$ and that the point falls above the curve for the associated value of \hat{D} , then there will not be a steady state solution. It is for this reason that large N_0 and large Q resulted in singularities in figure 6. Part of the reason that we find a region of parameter space that does not have a steady state is that we have neglected mass conservation, i.e., equation (5), by assuming that $q=Q/(2\pi r)$ and neglecting the right hand side of this equation. As the melt rate increases, due to larger Q or dN/dr, this approximation is no longer viable.

3.2.2 Flux solution

As we saw in the last section, ignoring basal melt around the borehole and fixing $q = Q/(2\pi r)$ can produce unphysical pressures at the origin at high extraction fluxes. Relatedly, for small values of the extraction flux, we would expect all the extracted water to be sourced from basal melt in a small area around the borehole, while the fixed flux solution (i.e., $q = Q/(2\pi r)$) overestimates the radius of influence by imposing an inwards flux everywhere in the domain. Both of these drawbacks are illustrated in figure 8. To ameliorate these issues, in this section, return to a fuller axisymmetric solution where we explicitly solve for the flux q as a function of the radius r using mass conservation.

We scale all the variables as in equations (11)-(13) and the flux as

$$q = \frac{Q}{2\pi r_d} q^*.$$

300

We also add in a nondimensional version of mass conservation, equation (5), which gives the steady state system of equations

$$Mq(1+Rq) = -b^3 \frac{dN}{dr},\tag{31}$$

 $\dot{m} = 1 - Dq \frac{dN}{dr},\tag{32}$

$$\dot{m} = N^3 b,\tag{33}$$

$$\frac{1}{r}\frac{d}{dr}(rq) = -W\dot{m}.\tag{34}$$

The minus sign in the last equation indicates that q is an extraction flux, i.e. flow is towards the borehole. Adding in mass conservation introduces a new parameter W, which is given by

$$W = \frac{2\pi \left(G + u_b \tau_b\right) r_d^2}{\rho_w \mathcal{L} Q} = \frac{N_0}{\rho_w \mathcal{L} D},$$

the ratio between meltwater produced in the domain and the flux extracted. We expect our previous solution to be a good approximation in the case of small W.

We solve these equations using a root-finding algorithm to find dN/dr and a shooting method to find N. At the nondimensional innermost point in the domain $r = r_i$, we impose $q = 1/r_i$ and guess the value of N. We then integrate to the nondimensional outermost point in the domain r = 1 and check if N = 1. Warburton et al. (2024) used a similar method to solve for the background state in their hydrology model.





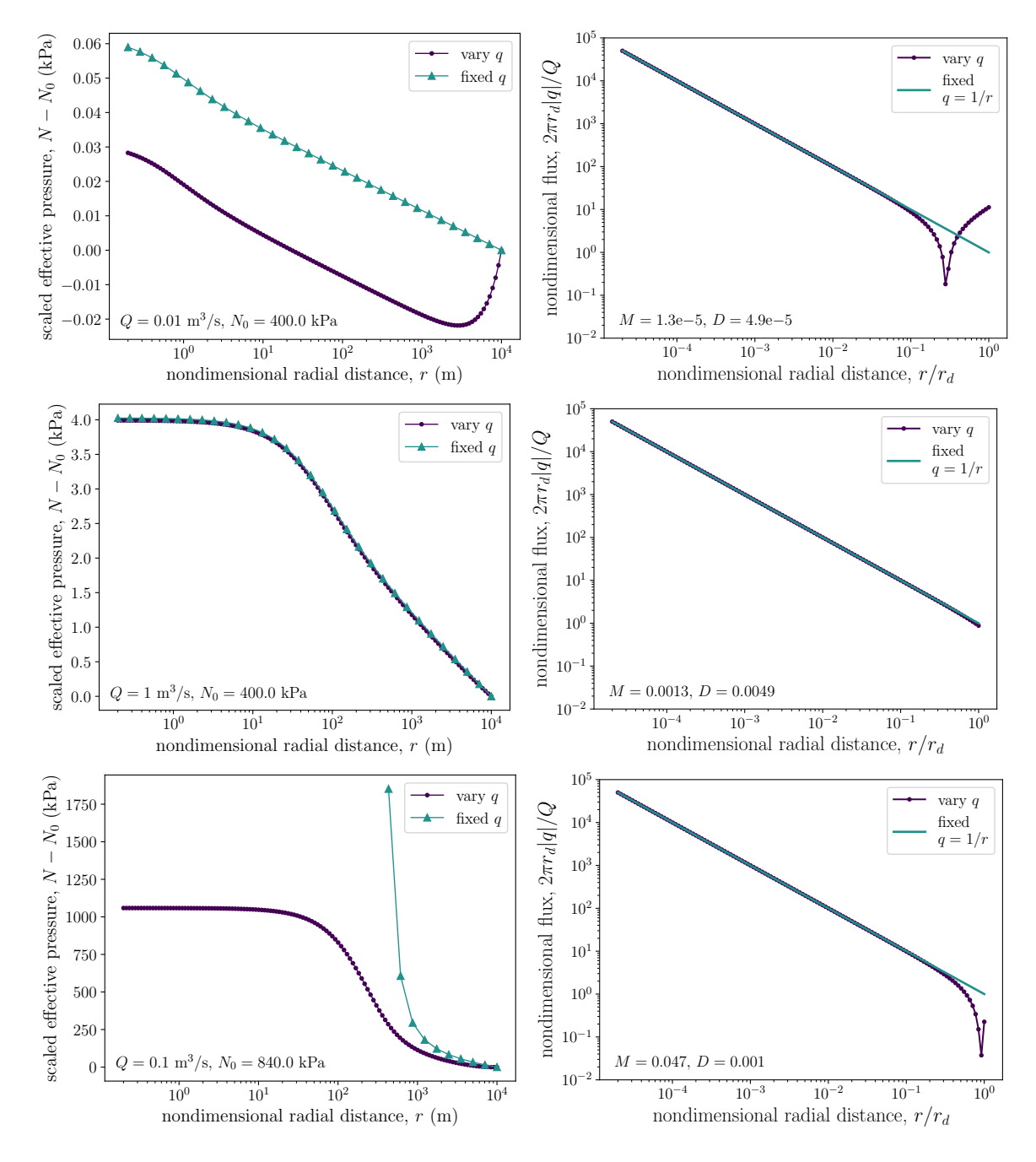


Figure 8. Comparison between the fixed flux (i.e., $q = Q/[2\pi r]$) solutions and the varying flux model. The left column shows the effective pressure $N-N_0$ with radius r and the right column shows the flux q with r. There are three parameter regimes: (top) low flux and moderate N_0 , which shows a flow reversal near the outer boundary that influences effective pressure throughout the domain; (middle) larger flux with moderate N_0 , here the solutions are nearly identical, with hint of lowering at the outer edge of the domain; and (bottom) low flux with a large effective pressure, leads to a singularity within the domain for the fixed flux and a regular solution for the varying flux model.



320



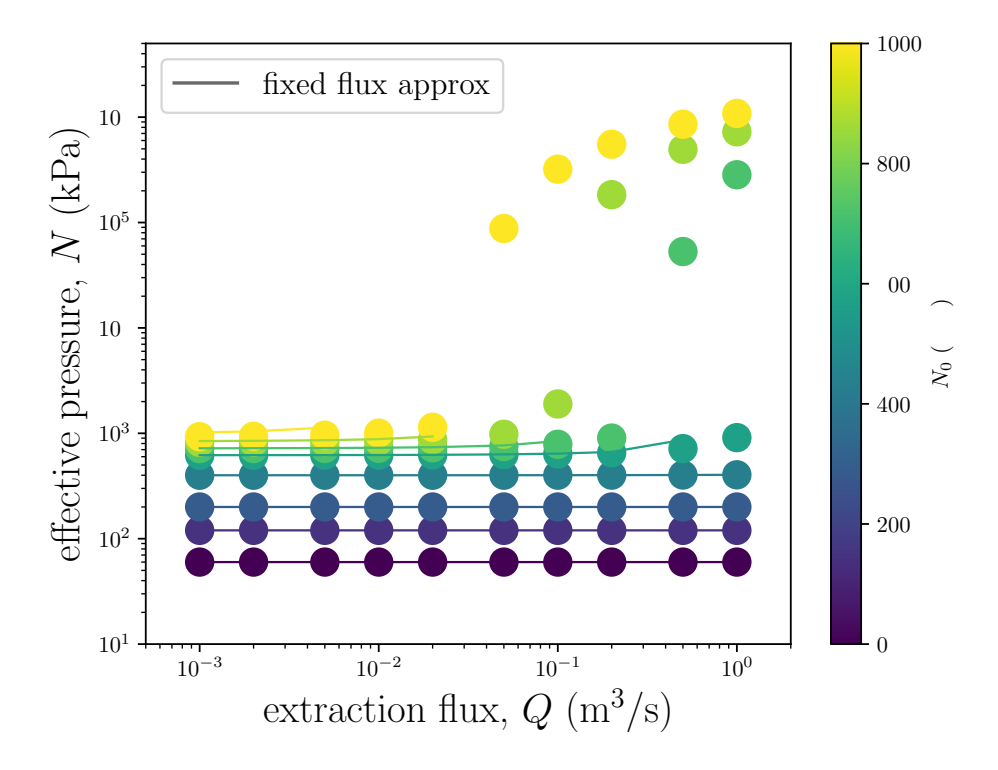


Figure 9. Varying flux solution for the effective pressure at the water extraction location, cf. figure 6. Each dot represents a simulation with a particular Q and N_0 . The outer radius here is 10 km. The colored curves are the fixed flux approximate solutions from equation (29), which do not yield a solution for large fluxes at high effective pressure.

In figure 8, we show solutions for the varying flux model and compare it to the fixed flux model. We distinguish between the three regimes, where (i) W is large since the flux Q is small, so the varying flux model captures the flow reversal in the outer part of the domain, (ii) the two models agree for moderate flux (W is small), and (iii) W is large since the effective pressure N_0 is large, and the the varying flux model converges whereas the fixed flux model diverges.

By solving for the flux using this method, we can more realistically capture the effective pressure at the water extraction site for a wider regime of extraction fluxes Q and background effective pressures N_0 , which we show in figure 9. This plot is analogous to figure 6, except that it is for the varying flux model. We see that the varying flux model produces consistently slightly smaller effective pressures than the fixed flux model, but is able to capture the large effective pressure perturbations at high values of Q and N_0 , where previously (on 6) there was a solution breakdown. Away from this regime, the colored curves, which show the approximate solution from equation (29), agree well with the varying flux model for small N_0 and all Q as well as large N_0 and small Q, as in figure 8. For these steady state results, we find that the effective pressure at the extraction site depends on Q and N_0 , with larger values of each parameter producing a larger pressure spike. If, however, the extraction flux or the effective pressure is small, the effective pressure is dominated by the background flow. This is important for connecting the results of the simplified axisymmetric model to the full SHAKTI simulations. In the next section, we consider the timescale





for the effective pressure to equilibrate to this steady state. In the following section, we analyze the time-dependent, coupled evolution of subglacial sliding at Helheim in SHAKTI-ISSM.

4 Influence on ice velocity at Helheim Glacier

We now return to the SHAKTI-ISSM simulations that sparked our interest in the axisymmetric problem: water extraction from Helheim Glacier, Greenland, where we use the same model and sliding law as described in section §2. The question we aim to answer here is: what effect on velocity does this pumping strategy of multiple sites produce, compared to a single extraction site? We start by understanding the transient dynamics.

4.1 Time to steady state and extraction at the confluence

A pertinent question is how long is required for the subglacial system to respond fully to water extraction. From the timedependent version of SHAKTI (equation (2); Sommers et al., 2018), the gap height evolves according to

$$\frac{\partial b}{\partial t} = \frac{\dot{m}}{\rho_i} - AN^3b,\tag{35}$$

where opening is caused by melt and closing is due to creep of the ice. In steady state, the two terms on the right are balanced, so that as steady state is approached both terms will have the same scaling, as described in section 3. We find that the time to steady state is likely controlled by the creep closure timescale, i.e.,

340
$$[t] \sim \frac{1}{AN^3},$$
 (36)

where the brackets around t indicate that it is a scaling. Taking a representative effective pressure value of $N_0 \sim 1000$ kPa and the ice softness $A \simeq 3.5 \times 10^{-25}$ Pa $^{-3}$ s $^{-1}$, the response timescale is on the order of

$$[t] \sim 33$$
 days.

350

For a range of initial effective pressure values from 100 – 2000 kPa, the time scale to reach steady state varies from 90 years to 4 days, with higher effective pressure corresponding to shorter response time. We expect that this scaling for time will also apply to the time for the system to recover (or "heal") following cessation of water extraction.

To examine these response times quantitatively, we performed a simulation over 270 days, with pumping at a steady rate of $Q = 1 \text{ m s}^{-1}$ applied at the confluence extraction site at Helheim during days 90-180, in order to clearly demonstrate the response to pumping and the subsequent healing following the pumping period. As shown in figure 10, the effective pressure at the pumping site exhibits a short adjustment response to initiation and cessation of pumping. The expected timescale [t] from equation (36) for this simulation is 1 hour, so it is unsurprising that the adjustment occurs quickly. Figure 10 also shows that the effective pressure returns to the same value after pumping. In figure 11, we show the change in effective pressure after 90 days of pumping. The largest impact is within a ring of about 2 km but variation in effective pressure is visible out to 5+km away. In this coupled SHAKTI-ISSM simulation, the hydrology affects the ice velocity, which is also show on figure 11.





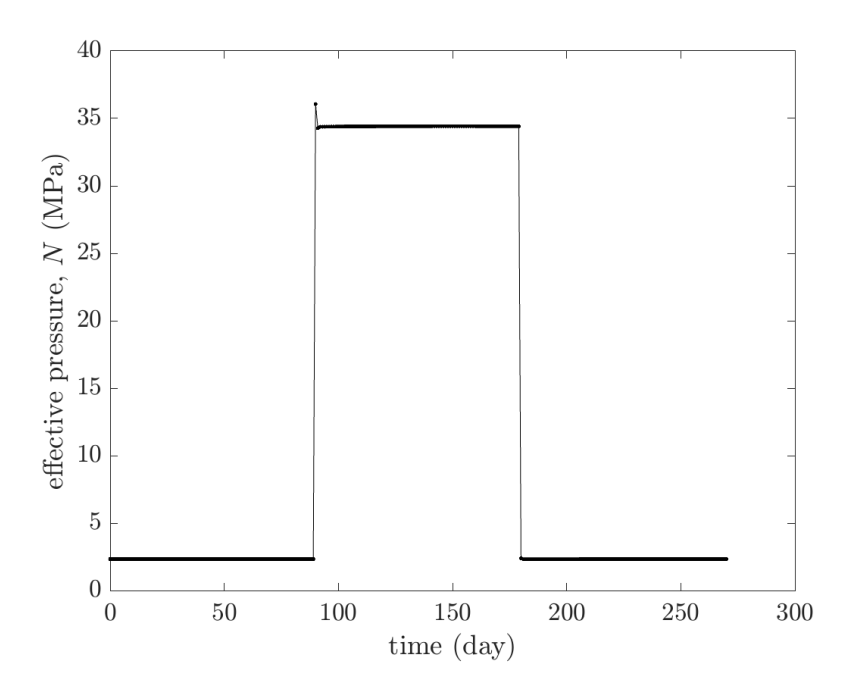


Figure 10. Change in effective pressure at the water extraction site over a pumping and recovery cycle at the "confluence point" of Helheim Glacier, Greenland (location shown in figure 11).

355 The 90-day water extraction at the confluence leads to a modest slowdown on the order of 1 meter per year throughout both branches. There are also a few patches of acceleration.

4.2 Water extraction from numerous sites

360

365

Due to the physical and numerical limitations of extracting a large flux of water from a single borehole, we decided to extract water $Q = 1 \text{ m}^3/\text{s}$ at 11 sites in the same 270-day pumping-and-healing experiment setup described in the previous section, with pumping employed during days 90-180, which we call the 'pumping strategy'. Starting from the winter background state (i.e., no external water inflow, where all water at the bed is produced through basal melt), we then extract water from these 11 boreholes and allow the glacier velocity and subglacial hydrology to evolve in time, as shown in figure 13. The selected points are shown in figure 12. These points were chosen arbitrarily to be distributed along both branches and the main trunk of the glacier. There is intended overlap between some of these points and the locations analyzed by Sommers et al. (2024), where those authors show that terminus effects propagate \sim 15 km upstream at Helheim. In the simulations here, neither the pumping strategy nor the location of the individual extraction sites were optimized to give the largest velocity change; we leave this type of detailed strategy design to future work.

We find that this pumping strategy and model set up produce about 100 m/yr slowdown in the main trunks of Helheim, as shown in figure 12. As a fraction of the total velocity, this is a minor influence on the order of 0.5-1 % of the background



380

385



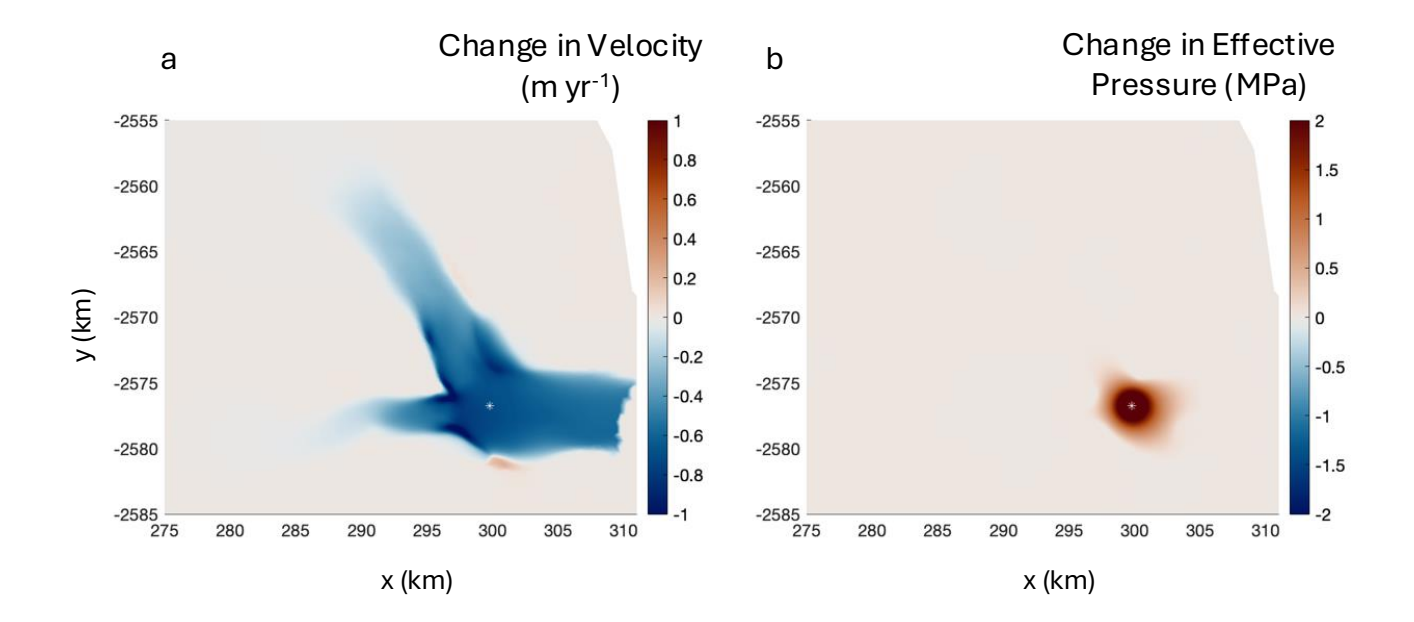


Figure 11. Pumping tests in the confluence region of Helheim Glacier, Greenland: (a) change in glacier velocity after 90 days of pumping at a rate of 1 m 3 s $^{-1}$, and (b) change in effective pressure. The white asterisk indicates the location of the extraction site.

velocity. We also only see deceleration, i.e., nowhere in the domain accelerates. In the discussion section §5, we highlight areas of future work including longer simulations runs, seasonal effects, and pumping strategy optimization. For now, as a first test of the possibility of pumping water out to slow a glacier (as described by the model physics we incorporated), we can say that such an approach does yield a modest velocity reduction.

In figure 13, we show the evolution of effective pressure with time for four representative sites. As at the confluence site, the effective pressure returns to the same value as before pumping, indicating that pumping did not cause noise-induced drift (Robel et al., 2024). Some of the sites, however, do show evolution in the effective pressure during pumping. At one of the locations in the main trunk we see a distinct transition in the effective pressure, indicative of a reconfiguration of the drainage network at that site caused by the water flow due to pumping, as shown in figure 12. At the far upstream site, the effective pressure oscillates before equilibrating to the a new steady state. These waves persist under time and space refinement, suggesting that they are not numerical artifacts but a transient reorganization of the drainage system. At other sites, a spike in effective pressure is apparent (i.e., figure 13), which is indicative of the constant gap height solution, as discussed in §3.1.1 and figure 3. The fast ice motion results in a large amount of meltwater generation at a large effective pressure, resulting in an unchanging gap height at some locations in the main trunk of Helheim (e.g., figure 12. In practice, this gap height remains fixed at the minimum allowable value imposed in the model and highlights the need for improved models of this critical component of glacier systems under low-flux conditions.





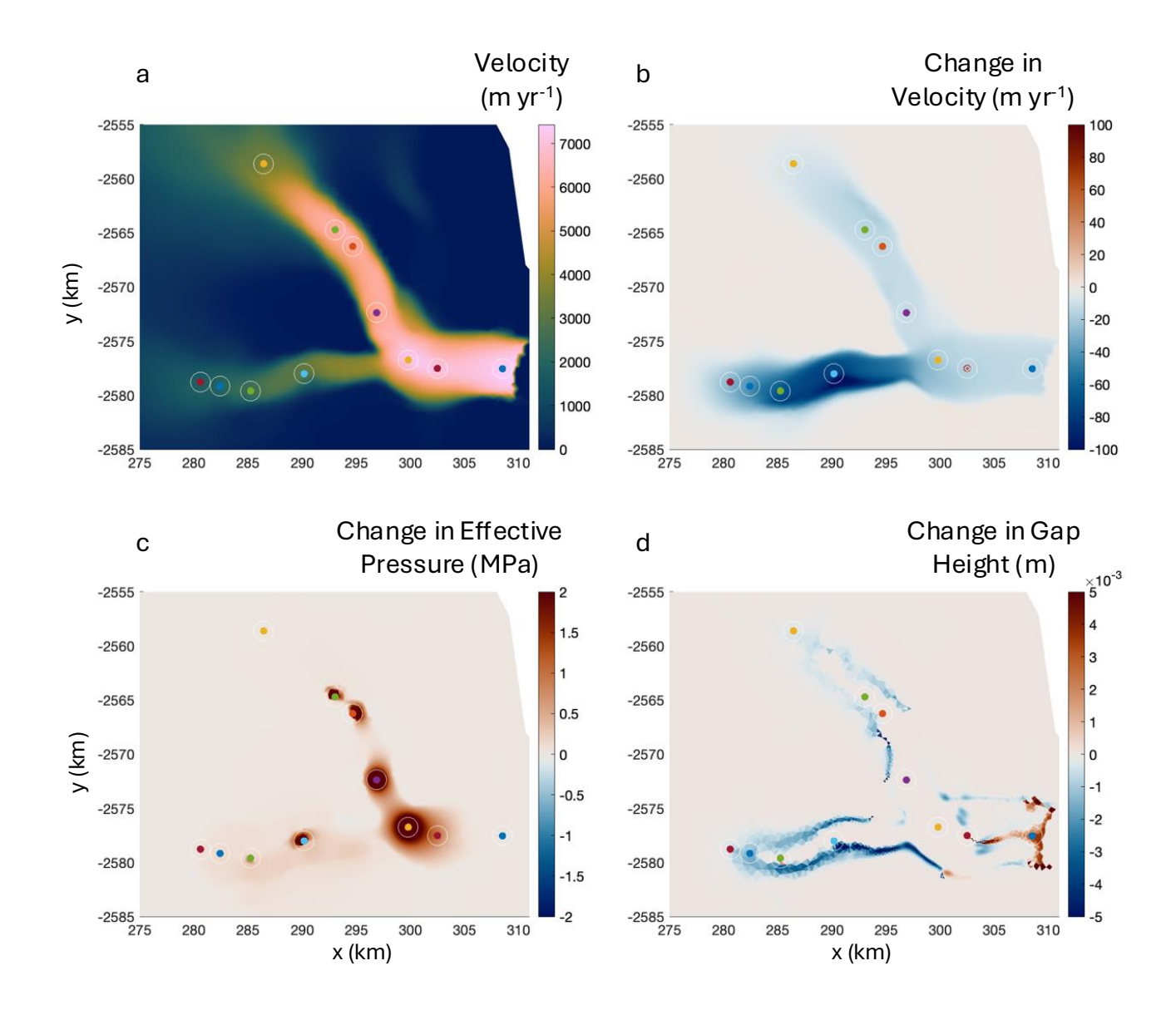


Figure 12. Pumping tests on Helheim Glacier, Greenland: (a) location of 11 extraction sites overlaid on initial glacier velocity, (b) change in ice velocity after 90 days of pumping at a rate of 1 m 3 s $^{-1}$ at each site, (c) change in effective pressure after 90 days of pumping, and (d) change in subglacial gap height after 90 days of pumping.





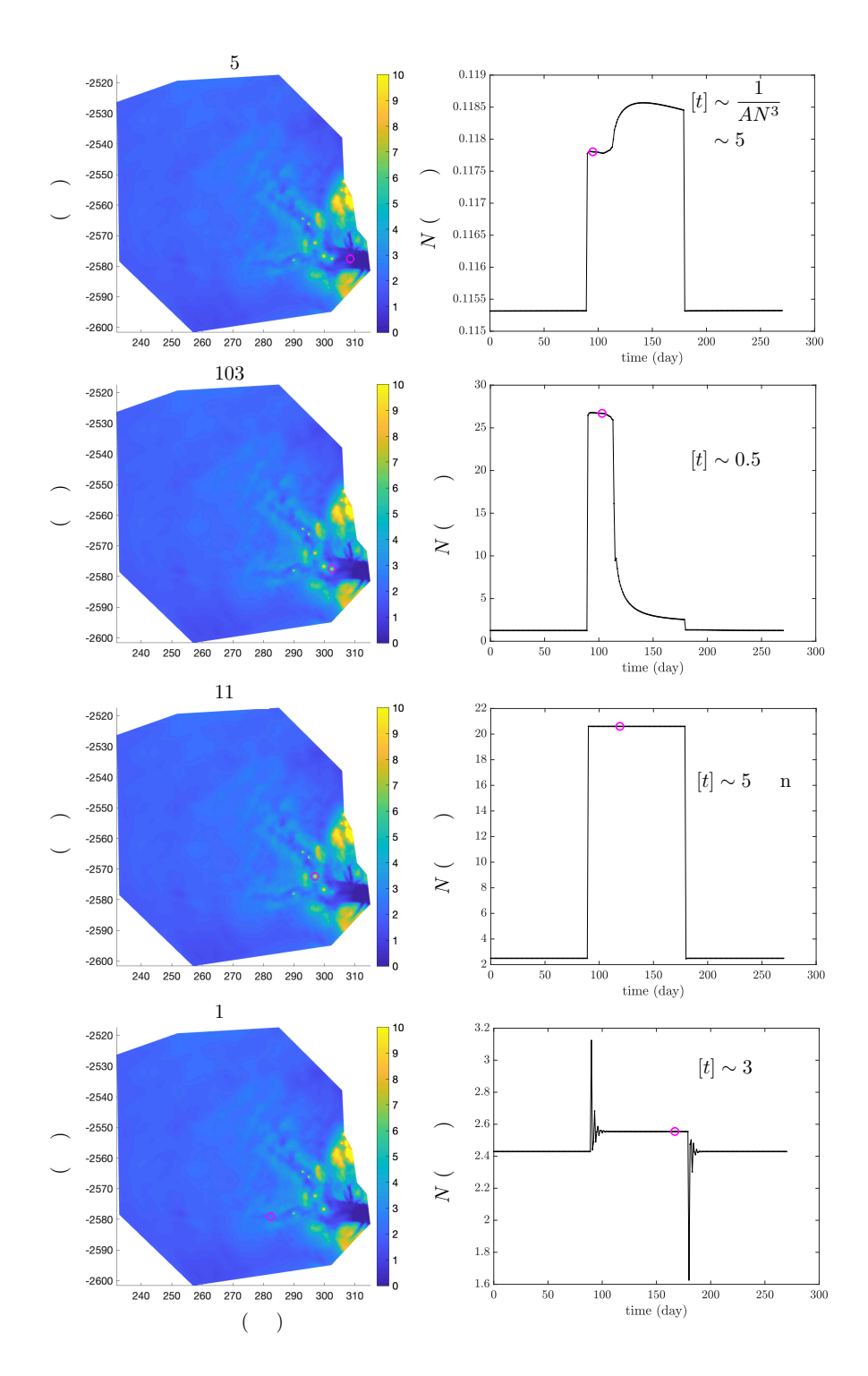


Figure 13. Change in effective pressure at 4 representative water extraction sites over a pumping and recovery cycle at Helheim Glacier. The left column shows the site locations at 4 times during the extraction period. The right column shows the effective pressure at the extraction site over time.





5 Discussion

390

395

400

405

410

415

In the context of using water extraction as a method to learn more about subglacial hydrology, our results provide predictions for the time to steady state, the effective pressure at the extraction site, and radius of influence. These predictions could be used in the design of laboratory and field experiments involving numerous boreholes spaced out radially, with water extracted from a from central borehole. The measured effective pressure distribution would allow us to compare the shape of the curve to our prediction and determine the parameters for the best-fit values of D, M, W, and R. It is also possible that these experiments could demonstrate that our model does not contain the dominant physics, and the radial distribution of effective pressure could take a different form. This outcome would result in a helpful reformulation of subglacial hydrology and provide context for comparison to experiments, similar to the determination of effective film thickness by Engelhardt and Kamb (1997).

In our predictions for the effect of water extraction on glacier velocity, we ignored seasonal dynamics (e.g., surface meltwater draining to the bed), as well as multi-year impacts, and we did not optimize the location of the extraction points. While we leave these extensions to future work, it is worth discussing how they may affect the results. First, the seasonal water input from surface melting at Helheim is immense (on the order of 1 km³; Stevens et al., 2022a) and water extraction would have a difficult time competing: it would take \sim 32 years for a single borehole with $Q=1~{\rm m}^3/{\rm s}$ to extract the surface melting of a single season. In future simulations, we will include surface water input and examine the most effective time period to pump. It is clear that the pumping strategy affects the relationship between water extraction and glacier slowdown, yet the simulations presented here were intended to be illustrative of the overall concept and we did not optimize the locations of extraction, the timing, or the pumping rate. For example, all of the locations in the main trunk of Helheim have only a small effect on the resulting velocity (cf. figure 12). This makes sense given the Sommers et al. (2024) results, where they showed that hydrology is most influential in the upstream regions. On longer time scales, i.e., over repeated seasons of water extraction, feedbacks related to sliding and freezing to the bed could kick in. Water piracy is hypothesized to be the cause of the Kamb Ice Stream stagnation in Antarctica (e.g. Alley et al., 1994) and could affect the long-term evolution of Helheim as water is extracted. Freezing to the bed due to slowing glacier velocity would be more effective at reducing glacier flux than extracting water alone. In further research, we plan to optimize locations of water extraction (focusing on the upstream reaches), incorporate seasonal dynamics, and run multi-year simulations.

In this work, we did not consider the practical question that arises of what happens to the extracted water. Possibilities include making snow (during winter pumping when air temperatures are consistently below freezing) or injecting the extracted water down an existing moulin (during a summer deployment), aiming to enhance an existing efficient subglacial channel, draining pressure from the surrounding bed. Nor did we consider the energetics or engineering considerations for such a pumping strategy to be implemented, the cost-benefit analysis, or the ethical and moral considerations of such an approach. This we leave for future studies, for which this present work may provide some constraints on the scale of intervention required.

As a glacier intervention strategy, our results suggest that water extraction can act to moderately slow fast-moving glaciers, and that more research is required. Attainable pumping rates over a field-season time span, with a drilling campaign that has precedent in the literature (e.g. Kamb, 2001), in a model that encodes our knowledge of ice and water flow physics, results in a





small slowdown of Helheim Glacier, one of the fastest-flowing glaciers on planet Earth. As expected, water extraction did not stop Helheim in its tracks. However, the results are promising and more research is required to understand the mechanics by which water extraction could slow a glacier. In this paper, we focused on simulations of Greenland, building on existing model configurations. However, considering the physics of glacier intervention in Greenland holds clear drawbacks: large amounts of surface meltwater and rapid glacier flow. Thwaites Glacier in West Antarctica, which is far more important for sea-level rise, flows more slowly and does not currently produce surface melt. In future simulations, we will assess how water extraction affects Thwaites' velocity to test whether it is more impactful in that setting than at Helheim. If we find that water extraction is only modestly effective, the research spurred by this line of inquiry will still improve subglacial hydrology models and therefore sea-level rise projections.

6 Conclusions

Changes in subglacial water flux and pressure affect glacier velocity. In this paper, we analyzed the effects of water extraction on glacier velocity. We started by considering axisymmetric subglacial water flow around a single borehole. We found an approximate analytical solution and used this framework to answer three key questions about the propagation distance, the extraction pressure, and the time scale of evolution. We found that the effective pressure perturbations had a logarithmic component, allowing the effective pressure to stay elevated far away from the borehole. We determined the relationship between extraction flux and extraction effective pressure. We showed that creep closure dominates the time it takes for the pumping to reach steady state and similarly recover following pumping, with typical response times on the order of days. Building off these results, we presented coupled subglacial hydrology—ice dynamics simulations of Helheim Glacier, Greenland using the coupled model SHAKTI-ISSM. We found modest velocity reductions for a short but reasonable pumping strategy. In aggregate, we find that there is great utility in studying water extraction as a way to learn more about the subglacial hydrologic system and determine its efficacy as a glacier intervention strategy.

Code availability. Code and analysis scripts for the SHAKTI-ISSM simulations as well as solutions to the fixed and variable flux problems can be found at https://github.com/colinrmeyer/water-extraction. We will add a public-release Zenodo doi after review.

Appendix A: Asymptotic solution for a small extraction flux

In section 3.2.2, we observed that for small extraction fluxes, that fluid can enter from the outer edge of the domain. We can describe these dynamics in the asymptotic limit of a small extraction flux and ignore dissipation, i.e. $M \ll 1$, $R \ll 1$, $W \gg 1$,





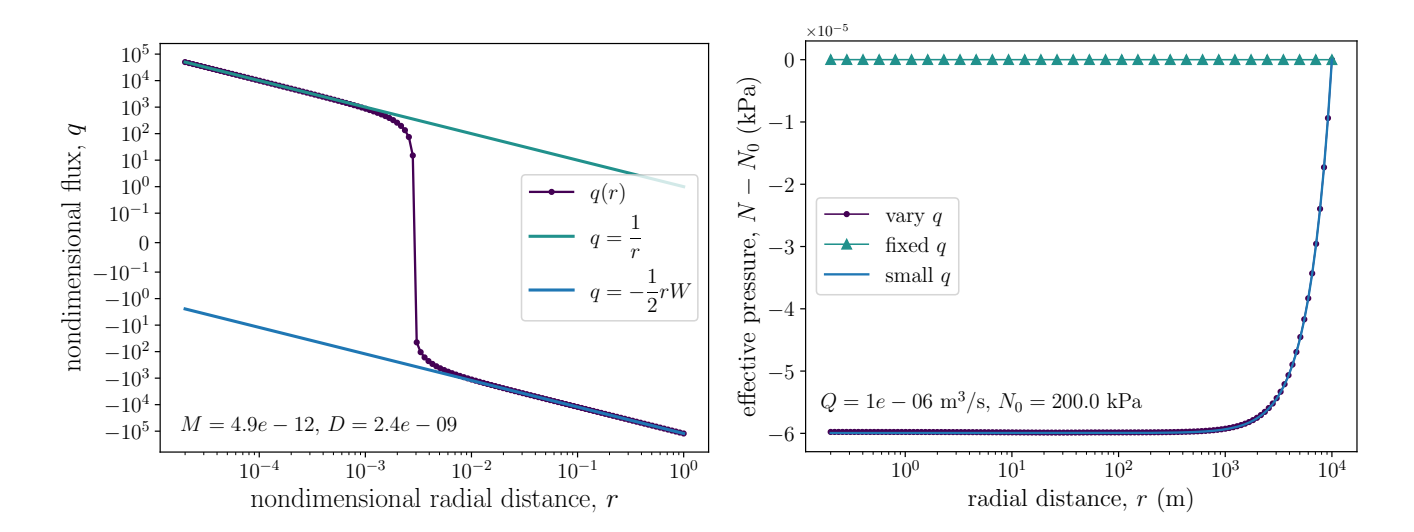


Figure A1. Asymptotic solution for a small extraction flux: (left) flux with distance, showing a transition to the small q solution. (right) the small flux solution for the effective pressure agrees with the full solution.

and D=0. In this distinguished limit, we can reduce equations (31)-(34) to

$$Mq(1+Rq) = -N^{-9}\frac{dN}{dr},\tag{A1}$$

$$\frac{1}{r}\frac{d}{dr}(rq) = -W. \tag{A2}$$

We now integrate mass conservation to determine the flux as

450
$$q = -\frac{1}{2}Wr,$$
 (A3)

where we take the constant of integration that comes from setting the inner boundary condition to be zero, since W is large. Inserting the flux into equation (A1), we find that

$$-4MWr + 2RW^2Mr^2 = \frac{d}{dr}\left(N^{-8}\right). \tag{A4}$$

Integrating and applying the outer boundary condition, N = 1 at r = 1, gives

455
$$N = \left[1 + 2MW(1 - r^2) - \frac{2}{3}RW^2M(1 - r^3)\right]^{-1/8},$$
 (A5)

which is shown in figure A1. The asymptotic model agrees with the full flux model. The minimum effective pressure is given by

$$N_{\min} = \left[1 + 2MW - \frac{2}{3}RW^2M \right]^{-1/8}.$$
 (A6)



480



This solution works well for small fluxes, as shown in figure A1. The dimensionless groups that arise in this solution are given by

$$MW = \frac{12\mu r_d}{[b]^3N_0}\frac{\left(G + u_b\tau_b\right)r_d}{\rho_w\mathscr{L}} \quad \text{and} \quad RW^2M = \frac{12\omega\rho_i\rho_w\mathscr{L}A^3N_0^8r_d^3}{\left(G + u_b\tau_b\right)},$$

which are independent of the flux Q. The first group can be seen as a ratio of the flux generated from melting due to sliding and geothermal heat to the expected flux through the system. The second term determines the role of turbulent melting in the system as compared to geothermal heat and sliding.

Returning to the step above where we set the inner boundary condition to zero, this choice is not required and we can derive a more general analytical solution by including the inner flux. In this way, we find that

$$q = -\frac{1}{2}Wr + \frac{1}{r}. (A7)$$

Inserting this flux into equation (A1), we find that

$$\frac{M}{r} + \frac{MR}{r^2} - MWR - \frac{1}{2}rWM + \frac{1}{4}r^2MW^2R = \frac{1}{8}\frac{d}{dr}\left(N^{-8}\right). \tag{A8}$$

470 Upon integrating and applying the outer boundary condition, we find that

$$N = \left\{ 1 + 8M \left[\ln\left(r\right) + R\left(1 - \frac{1}{r}\right) + WR(1 - r) + \frac{1}{4}W\left(1 - r^2\right) - \frac{1}{12}W^2R\left(1 - r^3\right) \right] \right\}^{-1/8},\tag{A9}$$

which is a combination of the earlier analytical solution that neglects dissipation, i.e. equation (20), and the small-flux asymptotic solution just described, equation (A5). This solution extends the applicability of the small flux asymptotics to larger values of M, R, and smaller values of W.

475 Author contributions. CRM: conceptualization, analysis, methodology, original draft preparation, funding acquisition. KLPW: conceptualization, analysis, methodology, review and editing. ANS: conceptualization, analysis, methodology, review and editing. BMM: conceptualization, review and editing, funding acquisition.

Competing interests. The authors declare that they have no conflict of interest. CM and BM are co-founders of Arête Glacier Initiative (areteglaciers.org), a non-profit organization that is fiscally sponsored by Digital Harbor Foundation. Arête was founded in 2024 to provide funding to glaciological research community focused on sea-level rise. BM and CM's consulting work with Arête is separate from their university research activities. They declare no financial, personal, nor professional conflicts of interest.

Acknowledgements. We thank Alan Rempel, Aaron Stubblefield, Ken Mankoff, Doug MacAyeal, Ethan Pierce, and Christine Dow for insightful conversations. This work was funded by the Grantham Foundation.





References

500

- 485 Alley, R. B.: Towards a hydrological model for computerized ice-sheet simulations, Hydrological Processes, 10, 649–660, https://doi.org/https://doi.org/10.1002/(SICI)1099-1085(199604)10:4<649::AID-HYP397>3.0.CO;2-1, 1996.
 - Alley, R. B., Blankenship, D. D., Bentley, C. R., and Rooney, S. T.: Deformation of till beneath ice stream B, West Antarctica, Nature, 322, 57–59, https://doi.org/10.1038/322057a0, 1986.
- Alley, R. B., Anandakrishnan, S., Bentley, C. R., and Lord, N.: A water-piracy hypothesis for the stagnation of Ice Stream C, Antarctica, Ann. Glaciol., 20, 187–194, https://doi.org/10.1017/S0260305500016438, 1994.
 - Andrews, L. C., Catania, G. A., Hoffman, M. J., Gulley, J. D., Lüthi, M. P., Ryser, C., Hawley, R. L., and Neumann, T. A.: Direct observations of evolving subglacial drainage beneath the Greenland Ice Sheet, Nature, 514, 80–83, https://doi.org/10.1038/nature13796, 2014.
 - Brinkerhoff, D. J., Meyer, C. R., Bueler, E., Truffer, M., and Bartholomaus, T. C.: Inversion of a glacier hydrology model, Ann. Glaciol., pp. 1–12, https://doi.org/10.1017/aog.2016.3, 2016.
- 495 Carey, M., Barton, J., and Flanzer, S.: Glacier protection campaigns: what do they really save?, in: Ice humanities, pp. 89–109, Manchester university press, https://doi.org/10.7765/9781526157782.00012, 2022.
 - Creyts, T. T. and Schoof, C.: Drainage through subglacial water sheets, J. Geophys. Res., 114, 1–18, https://doi.org/10.1029/2008jf001215, 2009.
 - Das, S. B., Joughin, I., Behn, M. D., Howat, I. M., King, M. A., Lizarralde, D., and Bhatia, M. P.: Fracture Propagation to the Base of the Greenland Ice Sheet During Supraglacial Lake Drainage, Science, 320, 778–781, https://doi.org/10.1126/science.1153360, 2008.
 - de Fleurian, B., Werder, M. A., Beyer, S., Brinkerhoff, D. J., Delaney, I., Dow, C. F., Downs, J., Gagliardini, O., Hoffman, M. J., Hooke, R. L., et al.: SHMIP The subglacial hydrology model intercomparison Project, J. Glaciol., 64, 897–916, https://doi.org/10.1017/jog.2018.78, 2018.
- Dow, C. F., Ross, N., Jeofry, H., Siu, K., and Siegert, M. J.: Antarctic basal environment shaped by high-pressure flow through a subglacial river system, Nat. Geosci., 15, 892–898, https://doi.org/10.1038/s41561-022-01059-1, 2022.
 - Doyle, S. H., Hubbard, B., Christoffersen, P., Law, R., Hewitt, D. R., Neufeld, J. A., Schoonman, C. M., Chudley, T. R., and Bougamont, M.: Water flow through sediments and at the ice-sediment interface beneath Sermeq Kujalleq (Store Glacier), Greenland, J. Glaciol., 68, 665–684, https://doi.org/10.1017/jog.2021.121, 2022.
- Ehrenfeucht, S., Dow, C., McArthur, K., Morlighem, M., and McCormack, F. S.: Antarctic Wide Subglacial Hydrology Modeling, Geophys.

 Res. Lett., 52, e2024GL111386, https://doi.org/https://doi.org/10.1029/2024GL111386, 2025.
 - Engelhardt, H., Humphrey, N., Kamb, B., and Fahnestock, M.: Physical conditions at the base of a fast moving Antarctic ice stream, Science, 248, 57–59, https://doi.org/10.1126/science.248.4951.57, 1990.
 - Engelhardt, H. F. and Kamb, B.: Basal hydraulic system of a West Antarctic ice stream: Constraints from borehole observations, J. Glaciol., 43, 207–230, https://doi.org/10.1017/S0022143000003166, 1997.
- 515 Engelhardt, H. F. and Kamb, B.: Basal sliding of Ice Stream B, West Antarctica, J. Glaciol., 44, 223–230, https://doi.org/10.1017/S0022143000002562, 1998.
 - Fitts, C. R.: Groundwater science, Elsevier (London), 2002.
 - Flamm, P. and Shibata, A.: 'Ice sheet conservation' and international discord: governing (potential) glacial geoengineering in Antarctica, International Affairs, 101, 309–320, https://doi.org/10.1093/ia/iiae281, 2025.





- Flowers, G. E.: Modelling water flow under glaciers and ice sheets, Proc. R. Soc. Lond. Ser. A, 471, https://doi.org/10.1098/rspa.2014.0907, 2015.
 - Hewitt, I. J.: Modelling distributed and channelized subglacial drainage: the spacing of channels, J. Glaciol., 57, 302–314, https://doi.org/10.3189/002214311796405951, 2011.
- Kamb, B.: Glacier surge mechanism based on linked cavity configuration of the base water conduit system, J. Geophys. Res., 92, 9083–9099, https://doi.org/10.1029/jb092ib09p09083, 1987.
 - Kamb, W. B.: Basal zone of the West Antarctic Ice Streams and its role in lubrication of their rapid motion, in: The West Antarctic Ice Sheet: Behavior and Environment, edited by Alley, R. B. and Bindschadler, R. A., vol. 77, pp. 157–199, AGU, Washington, DC, https://doi.org/10.1029/ar077p0157, 2001.
- Kyrke-Smith, T. M., Katz, R. F., and Fowler, A. C.: Subglacial hydrology and the formation of ice streams, Proc. R. Soc. Lond. Ser. A, 470, https://doi.org/10.1098/rspa.2013.0494, 2014.
 - Liljedahl, L. C., Meierbachtol, T., Harper, J., van As, D., Näslund, J.-O., Selroos, J.-O., Saito, J., Follin, S., Ruskeeniemi, T., Kontula, A., and Humphrey, N.: Rapid and sensitive response of Greenland's groundwater system to ice sheet change, Nat. Geosci., 14, 751–755, https://doi.org/10.1038/s41561-021-00813-1, 2021.
- Lockley, A., Wolovick, M., Keefer, B., Gladstone, R., Zhao, L.-Y., and Moore, J. C.: Glacier geoengineering to address sea-level rise: A geotechnical approach, Adv. Clim. Change Res., 11, 401–414, https://doi.org/https://doi.org/10.1016/j.accre.2020.11.008, 2020.
 - Mankoff, K. D., Solgaard, A., Colgan, W., Ahlstrøm, A. P., Khan, S. A., and Fausto, R. S.: Greenland Ice Sheet solid ice discharge from 1986 through March 2020, Earth Syst. Sci. Data, 12, 1367–1383, https://doi.org/10.5194/essd-12-1367-2020, 2020.
 - Mejía, J. Z., Gulley, J. D., Trunz, C., Covington, M. D., Bartholomaus, T. C., Xie, S., and Dixon, T. H.: Isolated cavities dominate Greenland ice sheet dynamic response to lake drainage, Geophys. Res. Lett., 48, e2021GL094762, https://doi.org/10.1029/2021GL094762, 2021.
- Mejía, J. Z., Gulley, J. D., Trunz, C., Covington, M. D., Bartholomaus, T. C., Breithaupt, C., Xie, S., and Dixon, T. H.: Moulin Density Controls the Timing of Peak Pressurization Within the Greenland Ice Sheet's Subglacial Drainage System, Geophys. Res. Lett., 49, e2022GL100058, https://doi.org/10.1029/2022GL100058, 2022.
 - Minchew, B. and Joughin, I.: Toward a universal glacier slip law, Science, 368, 29-30, https://doi.org/10.1126/science.abb3566, 2020.
- Moon, T., Joughin, I., Smith, B., van den Broeke, M. R., van de Berg, W. J., Noël, B., and Usher, M.: Distinct patterns of seasonal Greenland glacier velocity, Geophys. Res. Lett., 41, 7209–7216, https://doi.org/10.1002/2014GL061836, 2014.
 - Moon, T. A.: Geoengineering might speed glacier melt, Nature, 556, 436–437, https://doi.org/10.1038/d41586-018-04897-5, 2018.
 - Moore, J. C., Gladstone, R., Zwinger, T., and Wolovick, M.: Geoengineer polar glaciers to slow sea-level rise, Nature, 555, 303–305, https://doi.org/10.1038/d41586-018-03036-4, 2018.
- Narayanan, N., Sommers, A. N., Chu, W., Steiner, J., Siddique, M. A., Meyer, C. R., and Minchew, B.: Simulating Seasonal Evolution of Subglacial Hydrology at a Surging Glacier in the Karakoram, J. Glaciol., p. 1–26, https://doi.org/10.1017/jog.2025.10078, 2025.
 - Poinar, K., Dow, C. F., and Andrews, L. C.: Long-Term Support of an Active Subglacial Hydrologic System in Southeast Greenland by Firn Aquifers, Geophys. Res. Lett., 46, 4772–4781, https://doi.org/10.1029/2019GL082786, 2019.
 - Rempel, A. W., Meyer, C. R., and Riverman, K. L.: Melting temperature changes during slip across subglacial cavities drive basal mass exchange, J. Glaciol., 68, 197–203, https://doi.org/10.1017/jog.2021.107, 2022.
- Robel, A. A., DeGiuli, E., Schoof, C., and Tziperman, E.: Dynamics of ice stream temporal variability: Modes, scales, and hysteresis, J. Geophys. Res., 118, 925–936, https://doi.org/10.1002/jgrf.20072, 2013.



565

575



- Robel, A. A., Verjans, V., and Ambelorun, A. A.: Biases in ice sheet models from missing noise-induced drift, Cryosphere, 18, 2613–2623, https://doi.org/10.5194/tc-18-2613-2024, 2024.
- Schoof, C.: Ice sheet acceleration driven by melt supply variability, Nature, 468, 803–806, https://doi.org/10.1038/nature09618, 2010.
- 560 Schoof, C. and Mantelli, E.: The role of sliding in ice stream formation, Proc. R. Soc. A, 477, 20200 870, https://doi.org/10.1098/rspa.2020.0870, 2021.
 - Siegert, M., Sevestre, H., Bentley, M. J., Brigham-Grette, J., Burgess, H., Buzzard, S., Cavitte, M., Chown, S. L., Colleoni, F., DeConto, R. M., Fricker, H., Gasson, E., Grant, S., Gulisano, A., Hancock, S., Hendry, K., Henley, S., Hock, R., Hughes, K., and Truffer, M.: Safeguarding the polar regions from dangerous geoengineering: a critical assessment of proposed concepts and future prospects, Front. Sci., 3, 1527 393, https://doi.org/10.3389/fsci.2025.1527393, 2025.
 - Solgaard, A. M., Rapp, D., Nool, B. P. Y., and Hvidberg, C. S.: Seasonal Patterns of Greenland Ice Velocity From Sentinel-1 SAR Data Linked to Runoff, Geophys. Res. Lett., 49, e2022GL100 343, https://doi.org/10.1029/2022GL100343, 2022.
 - Sommers, A., Rajaram, H., and Morlighem, M.: SHAKTI: Subglacial Hydrology and Kinetic, Transient Interactions v1.0, Geosci. Model Dev., 11, 2955–2974, https://doi.org/10.5194/gmd-11-2955-2018, 2018.
- 570 Sommers, A., Meyer, C. R., Morlighem, M., Rajaram, H., Poinar, K., Chu, W., and Mejía, J.: Subglacial hydrology modeling predicts high winter water pressure and spatially variable transmissivity at Helheim Glacier, Greenland, J. Glaciol., p. 1–13, https://doi.org/10.1017/jog.2023.39, 2023.
 - Sommers, A. N., Meyer, C. R., Poinar, K., Mejía, J., Morlighem, M., Rajaram, H., Warburton, K. L. P., and Chu, W.: Velocity of Greenland's Helheim Glacier Controlled Both by Terminus Effects and Subglacial Hydrology With Distinct Realms of Influence, Geophys. Res. Lett., 51, e2024GL109168, https://doi.org/10.1029/2024GL109168, 2024.
 - Stevens, L. A., Behn, M. D., Das, S. B., Joughin, I., Noël, B. P. Y., Broeke, M. R., and Herring, T.: Greenland Ice Sheet flow response to runoff variability, Geophys. Res. Lett., 43, https://doi.org/10.1002/2016GL070414, 2016.
 - Stevens, L. A., Nettles, M., Davis, J. L., Creyts, T. T., Kingslake, J., Ahlstrøm, A. P., and Larsen, T. B.: Helheim Glacier diurnal velocity fluctuations driven by surface melt forcing, J. Glaciol., 68, 77–89, https://doi.org/10.1017/jog.2021.74, 2022a.
- 580 Stevens, L. A., Nettles, M., Davis, J. L., Creyts, T. T., Kingslake, J., Hewitt, I. J., and Stubblefield, A.: Tidewater-glacier response to supraglacial lake drainage, Nat. Commun., 13, 6065, https://doi.org/10.1038/s41467-022-33763-2, 2022b.
 - Vijay, S., Khan, S. A., Kusk, A., Solgaard, A. M., Moon, T., and Bjørk, A. A.: Resolving Seasonal Ice Velocity of 45 Greenlandic Glaciers With Very High Temporal Details, Geophys. Res. Lett., 46, 1485–1495, https://doi.org/10.1029/2018GL081503, 2019.
- Warburton, K. L. P., Meyer, C. R., and Sommers, A. N.: Predicting the Onset of Subglacial Drainage Channels, J. Geophys. Res., 129, e2024JF007758, https://doi.org/10.1029/2024JF007758, 2024.
 - Weertman, J. and Birchfield, G. E.: Subglacial water flow under ice streams and West Antarctic ice-sheet stability, Ann. Glaciol., 3, 316–320, https://doi.org/10.3189/S0260305500002998, 1982.
 - Werder, M. A., Hewitt, I. J., Schoof, C., and Flowers, G. E.: Modeling channelized and distributed subglacial drainage in two dimensions, J. Geophys. Res., 118, 1–19, https://doi.org/10.1002/jgrf.20146, 2013.
- Zwally, H. J., Abdalati, W., Herring, T., Larson, K., Saba, J., and Steffen, K.: Surface melt-induced acceleration of Greenland ice-sheet flow, Science, 297, 218–222, https://doi.org/10.1126/science.1072708, 2002.